Dynamic nuclear interference structures in the Coulomb explosion spectra of a hydrogen molecule in intense laser fields: reexamination of molecular enhanced ionization

Chelkowski, Szczepan; Bandrauk, André D.; Staudte, André; Corkum, Paul B.

Publisher's version / Version de l'éditeur:
https://doi.org/10.1103/PhysRevA.76.013405
Physical Review A, 76, 1, pp. 1-16, 2007-07-16

Dynamic nuclear interference structures in the Coulomb explosion spectra of a hydrogen molecule in intense laser fields: Reexamination of molecular enhanced ionization

Szczepan Chelkowski,[1,*] André D. Bandrauk,[1] André Staudte,[2] and Paul B. Corkum[2]
[1]*Laboratoire de Chimie Théorique, Faculté des Sciences, Université de Sherbrooke, Sherbrooke, Québec, Canada J1K 2R1*
[2]*National Research Council, 100 Sussex Drive, Ottawa, Ontario, Canada K1A 0R6*
(Received 2 June 2007; published 16 July 2007)

Several theoretical models are used to explain the origin of the recently observed (unexpected) spectral progression in the Coulomb explosion spectra of the hydrogen molecule photoionized by an intense ultrashort laser pulse. In the first ionization step the molecule loses its first electron and then the H_2^+ molecular ion dissociates. Next, at the intermediate stage of the dissociation process, a localized electron state is created from which the second ionization occurs at each laser half-cycle. It is shown that interference between a net-two-photon and a one-photon transition introduces a dynamic structure into the nuclear wave packet corresponding to this localized electron state which leads to the regular spectral progressions seen in the experiment. We confirm these spectral progressions using numerical simulations based on a time-dependent Schrödinger equation describing the exact three-body dynamics of H_2^+ in one dimension.

DOI: 10.1103/PhysRevA.76.013405 PACS number(s): 33.80.Rv, 33.80.Gj, 42.50.Hz

I. INTRODUCTION

Interaction of intense ($I > 10^{13}$ W/cm^2) laser fields with matter leads to many new multiphoton, nonperturbative phenomena such as high harmonic generation, generation of attosecond pulses and above threshold ionization (ATI) [1,2]. These important phenomena were first observed and interpreted in atomic gases. Molecules exposed to intense laser fields add a new perspective into the study of intense laser-matter interactions related to the entanglement of the electron and nuclear motion, often called dissociative ionization, which cannot be easily separated as it has been in the past for stationary perturbative phenomena with the help of the Born-Oppenheimer approximation [3]. Thus the additional molecular parameters such as internuclear distance lead to various phenomena specific to molecules like Above Threshold Dissociation [3,4] ATD. Most important inherently molecular aspects of intense laser-matter interaction show up in kinetic energy spectra of nuclear fragments originating from Coulomb explosion of photoionized molecules. If a molecule exposed to an intense laser field loses several electrons within the time interval so short that nuclei can be considered as frozen then (if sufficient number of electrons was lost within this short time interval) by measuring kinetic energies of charged nuclear fragments we can use a simple mapping procedure to reconstruct the vibrational (bound or dissociating) nuclear wave function from Coulomb explosion spectra. Such a procedure, called Coulomb Explosion Imaging (CEI), has been extensively studied both theoretically [5,6] and experimentally [1,7,8]. CEI seems to be of interest from the fundamental perspectives as one the most direct measurement of the absolute value of the nuclear wave function, i.e., the measured momenta of exploding charged fragments are directly related in a simple way to the probability distribution of nuclear positions just before the classical Coulomb explosion has been triggered by the rapid removal of few electrons.

Another typically molecular aspect of intense laser interaction with matter is related to the phenomenon called Enhanced Ionization (EI) or Charge-Resonance Enhanced Ionization (CREI). This process was thoroughly studied theoretically in symmetric molecules (like H_2^+, D_2^+) [11–17] and recently in nonsymmetric molecules as well [18]. So far very few experiments were performed directly on H_2^+ ions. Most experiments were performed using neutral H_2 molecules and H_2^+ ions were produced during the rise of the laser femtosecond laser pulse (40–140 fs). These pulses are usually focused to peak intensities of $\sim 10^{13}$–10^{15} W/cm^2 into the gas jet of unaligned H_2 or D_2 neutral molecules. Typically, the electrons are not ejected instantaneously at the equilibrium configuration as one would require in an ideal CEI procedure. The double ionization process of a hydrogen molecule usually occurs in three steps shown in Fig. 1. During the first step, taking place during the rise of the laser pulse, the first electron is ejected nearly instantaneously via tunnelling. This process prepares a nuclear wave packet nearly identical to the initial vibrational state of H_2 via a vertical Franck-Condon transition onto the H_2^+ ground σ_g state [9,10]. Next, the second part of the laser field envelope launches the dissociation of H_2^+ driven by the strong coupling between the σ_g and the lowest σ_u electronic surface of the molecular ion. Finally, the last electron is ejected at much larger internuclear distances than the equilibrium internuclear separation, as illustrated in Fig. 1 which shows these two steps for a H_2^+ molecule in intense laser fields. Surprisingly, it was discovered theoretically that for a dissociating H_2^+ ion there exists a critical distance R_c at which the molecular ionization rate exceeds the atomic rate by several order of magnitudes. The EI occurs when the electron wave function is well localized on one nuclei [11–17]. In an aligned H_2^+ along the laser field there are two such localized states which in the absence of the field are nearly degenerate at $R > 6$ a.u.. The enhanced ionization occurs from the higher, σ_+, up-hill, quasi-static electronic energy state [13,16] from which the force from the laser electric field and the force from neighboring nuclei add up leading to a much

*s.chelkowski@usherbrooke.ca

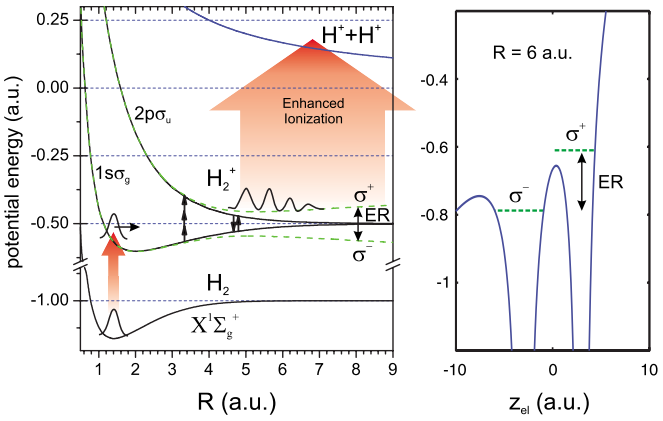

FIG. 1. (Color online) Sketch of the processes occurring in a H_2^+ intense laser field. The multiphoton or tunneling ionization of the first electron transfers populations from the ground state surface of a H_2^+ molecule to the the σ_g surface of H_2^+ (or D_2^+) and creates a wave packet that rapidly moves toward the outer turning point. The two dissociation pathways, net-two-photon (absorption of three photons and reemission of one photon) and one-photon, interfere on the quasistatic upper state. Enhanced ionization samples the population on this surface at the field maximum of each half laser cycle. Right panel shows the electronic potential as function of the electron coordinate z_{el} at the internuclear distance R=6 a.u. and the corresponding quasistatic levels $\sigma^{\pm}$. The second electron ionizes predominantly from the upper σ^+ state.

lower barrier to overcome or even to overbarrier ionization; see Fig. 1(b)). The ionization rate from the second lower state is much lower since the electron has a high and wide barrier to overcome. The Coulomb explosion spectrum will thus depend strongly on the R-dependence of the populations in this upper localized electron state. So far in the literature related to molecular EI it has been assumed that this population is smooth and constant or that the spectra are proportional to the total populations. In most previous investigations it was assumed that the Coulomb explosion spectra are directly proportional to the frequency dependent static ionization rate [17,19,20] calculated by solving a time-dependent Schrödinger equation (TDSE) for frozen nuclei and it was usually assumed that any dynamical R-dependent factor is irrelevant despite the fact that such a light molecule as H_2^+ dissociates with the speed of 1 a.u. per laser cycle. Clearly, after few laser cycles the nuclear wave packet undergoes a large change which means that predictions based on wavelength dependent ionization rates computed from TDSE for frozen nuclei are unreliable. More realistic is a new dynamic model we propose here based on the cumulative effect of instantaneous Coulomb explosions occurring at each laser half-cycle at maxima of the $|E(t)|$ field weighed by a corresponding DC rate and the shape of the wave packet obtained from a two-surface calculation.

In this work, we present a detailed analysis of the role of this nuclear wave packet factor, in the case of Coulomb explosion of H_2^+ and D_2^+, which is crucial for understanding of the experimental data reported earlier in [21]. Because of numerical limitations our theoretical work is limited to the dynamics of H_2^+ (or D_2^+) in an intense laser field. However, the experiment is performed by focusing the laser pulse on the neutral molecules. Therefore, an exact modelling would require to solve the H_2 two-electron (+ two-protons) problem. The measured Coulomb kinetic energy spectra of protons (or deuterons) show a regular progression in the sub-eV range. Our experimental technique [21] allowed to reveal these regular structures in the kinetic energy release (KER) of the Coulomb explosion spectra, for the first time. We suggested in [21] that this structure is related to population dynamics, as it occurs, when the dissociating wave packet evolves and traverses the EI region. The electron is ejected only at maxima and minima of the electric field via tunnelling or overbarrier ionization mechanisms. Thus the measured Coulomb explosion KER spectrum is a cumulative result of successive instantaneous Coulomb explosion imaging processes of the evolving wave packet. We show, by solving numerically the two-surface dynamics of the dissociating ion, that this wave packet has a very regular structure resulting from the interference between two possible dissociation pathways. The principal goal of this work is to establish theoretically, in more details than in the previous short letter [21], a link between the modulations in the experimental spectra and the spatial structure in the dissociating nuclear wave packet. Another goal is to explain the origin of this spatial structure. We show that this structure, dependent on the internuclear separation R, is directly determined, in a simple way, by the nuclear momenta of dissociating wave packets on the gerade (σ_g) and ungerade (σ_u) H_2^+ surfaces which in turn are related to the number of net-absorbed photons in the dissociation channel. In other words, our work completes previous theoretical investigations of EI in which this dynamic factor related to the wave packet shape has never been fully investigated. Other previous work on H_2^+ has also emphasized the importance of this quasi-static upper surface, called a doorway state [3,13,22]. Our work relates also to earlier experimental work [23,24] in which observed structures in KER Coulomb explosion spectra were attributed to the light-induced trapped state.

The paper is organized as follows: In Sec. II we briefly describe the experiment and the results; in Sec. III we compare the experimental Coulomb spectra for H_2^+ and for D_2^+ with theoretical spectra obtained from a numerical solution of TDSE describing the exact non-Born-Oppenheimer three-body dynamics in one dimension (electron and nuclei moving along one axis); in Sec. IV we investigate the interference structure in molecular wave packets obtained from the two-surface (σ_g and σ_u) dynamics; and in Sec. V we construct a simple Coulomb explosion model based on two-surface dynamics and DC-ionization rates. In this model the kinetic energy spectra are calculated as a sum of instantaneous Coulomb explosion at each laser half-cycle weighed by the DC-ionization rates corresponding to the electric-field value at each consecutive half-cycle, as shown in Fig. 1 (lower panel).

II. EXPERIMENTAL RESULTS

Femtosecond laser pulses (40–140 fs) of different wavelengths (800 nm, 1.2 μm, and 1.4 μm) were focused to peak intensities of $(1.0–4.5)\times 10^{14}$ W/cm^2 into the gas jet of un-

aligned H_2 and D_2. The peak intensity was determined using the radial electron and ion momentum of single ionization in circularly polarized light [25]. The uncertainty in the peak intensity is ≈10% at 800 nm and 30% at 1.2 μm and 1.4 μm. We determined the pulse duration using an SHG autocorrelator for all wavelengths with an uncertainty of ±10%.

Ions and electrons created in the focus are guided by electric and magnetic fields (23 V/cm, 12 G) towards two channel plate detectors with delay line position encoding. Ion momenta of up to 30 a.u. are collected with 4π solid angle. The electrons and ions were measured in coincidence which allowed to achieve an overall spectrometer momentum resolution of ±0.1 a.u. along and ±0.5 a.u. perpendicular to the spectrometer axis. Further details on the experimental setup can be found in [21,26].

The experimental KER spectra of protons or deuterons exhibit a sequence of spectroscopic lines which are formed during enhanced ionization (EI) of H_2 (or D_2) [11–13,17,18]. The lines appear for both linear and circular polarizations and at all wavelengths (800 nm–1.4 μm) and pulse durations (40–140 fs) that we have studied, see [21]. The peak positions are nearly intensity independent in the intensity range $I=10^{14}$ to 3×10^{14} W/cm^2. Whereas increasing intensity blurs the feature, it does not affect the line position. Although the overall structure of the spectral part associated with enhanced ionization curves change, there is always a spectral progression up to the intensity $I=3\times10^{14}$ W/cm^2. The peak positions (and the spacings between lines) depend on the wavelength and the isotope. The experiment shows that the lines positions shift to lower energies with increasing wavelength but the peak separations are rather slightly larger for longer wavelength (if compared in the similar energy range). The opposite should happen if the spacing were proportional to the photon energy. It also shows that the spacing between lines are smaller for a heavier isotope. The peak positions are, however, insensitive to a change of pulse duration (within a 40–140 fs range) but the line intensity is shifted from the high energy lines to the lower energetic lines when the pulse duration is increased.

In the next sections we reproduce these structures using the 1-D TDSE for H_2^+ and D_2^+. We also construct a simple model of the instantaneous Coulomb explosion occurring at subsequent laser half-cycles. The model describes the dissociation using the two-surface model. It allows us to establish the origins of the modulation appearing in the laser-molecule dynamics, more specifically, this model shows a link between the spatial structure of the wave packet and the observed experimental spectral lines.

III. EXACT THREE-BODY TDSE SIMULATIONS

The most rigorous and adequate, *ab-initio* theoretical approach to this experiment would require to solve the TDSE for a H_2 molecule, i.e. one should solve the time evolution problem involving the wave function depending on 9 spatial coordinates for two electrons and two nuclei, $4\times3-3$ (where 3 coordinates of the center of mass are subtracted), which is not feasible since the electron spatial grid should be sufficiently large in order to track the fast electron wave packets. Even if we restrict the nuclear motion to 1D (which may be a reasonable approximation for a non-rotating H_2 perfectly aligned with a linearly polarized laser electric field) we cannot numerically solve this 2-electron problem in its full dimensionality (i.e., 6 coordinates for the electrons+1-coordinate for the nuclear motion). Consequently, one is compelled to restrict the dynamics to the one-electron problem and one nuclear degree of freedom and one has to make an ad-hoc assumption about the initial state. One assumes usually that the first electron is instantaneously removed at a specific maximum or minimum of the laser electric field. Additionally, one assumes that a H_2^+ molecule is instantaneously created via a vertical Franck-Condon transition onto the H_2^+ σ_g state and at this moment our code starts to describe the dissociative ionization of H_2^+ or D_2^+. The validity of these assumptions and the corrections to this Franck-Condon transition model were discussed in [9,10,24].

After a turn-off of the laser pulse we project the final wave function on Coulomb nuclear continua and thus obtain the kinetic energy spectra of exploding nuclear fragments. We have already solved numerically in the past [27,28] the TDSE for a H_2^+ molecule aligned along the linearly polarized (along z-axis) laser electric field. Because of the symmetry this involves only two electron degrees of freedom (e.g the cylindrical coordinates ρ and z electron coordinate with respect to the center of mass of two nuclei) and internuclear separation R. So far, even for this reduced problem there are no reported converged calculations of Coulomb explosion spectra. The difficulty consists in the necessity to use extremely huge electron grids. To allow the use of smaller electron grids, in most calculations absorbing boundaries are introduced but unfortunately this leads to the loss of the electron flux after few electron cycles and consequently the Coulomb explosion spectra are affected by the use of an absorber. In [29] we have overcome in part this difficulty by using a wave function splitting technique which so far has been successfully used only for electron-proton motion in 1-D. It allows to recover the absorbed wave function which is next propagated in time using the exact Volkov propagator [29]. Results presented here are based on this technique.

We have solved numerically the complete, 3-body, 1-D, TDSE with both electronic and nuclear degrees of freedom included (in atomic units, $\hbar=m_e=e=1$)

$$i\frac{\partial\psi(z,R,t)}{\partial t}=[H_R(R)+V_C(z,R)+H_z(z)]\psi(z,R,t), \quad (1)$$

where z is the electron coordinate (with respect to the nuclear center of mass), R is internuclear distance, with corresponding electronic $H_z(z)$, nuclear $H_R(R)$ Hamiltonians,

$$H_z(z)=-\beta\frac{\partial^2}{\partial z^2}+\kappa zE(t), \quad H(R)=-\frac{1}{m_N}\frac{\partial^2}{\partial R^2}+\frac{1}{R}, \quad (2)$$

where

$$\beta = \frac{(2m_N + m_e)}{4m_N m_e}, \quad \kappa = 1 + \frac{m_e}{2m_N + m_e},$$

and the regularized Coulomb potential V_C originating from the two nuclei,

$$V_C(z,R) = \frac{-1}{\sqrt{(z-R/2)^2+1}} + \frac{-1}{\sqrt{(z+R/2)^2+1}}. \tag{3}$$

m_e and m_N are the electron and nucleus (proton or deuteron) masses. The Hamiltonian used in Eq. (1) is the *exact* three body Hamiltonian obtained after separation of the center-of-mass motion [29] in 1D. We solve the TDSE (1) numerically, using the method described in [29]. The initial wave function, at t=0 was assumed to be in the following form:

$$\psi(z,R,0) = \chi(R)\psi_g^0(R,z), \tag{4}$$

where $\psi_g^0(R,z)$ is the field-free eigenfunction of the molecular electronic Hamiltonian of H_2^+ at fixed R. We used (except in the case of Fig. 6) χ(R) equal to the vibrational ground state ($v=0$) of H_2 or D_2, shown in Fig. 1. This is equivalent to assuming that, during the ionization of H_2, the nuclei remained frozen and a direct vertical Franck-Condon-like transition from H_2 to H_2^+ takes place.

Since the most likely moment for the ionization of the first electron in H_2 is within few cycles around the peak of the pulse envelope, we use in our simulations an artificial laser pulse envelope [24] which rises from zero to its maximal value within the time $t_{\rm rise}=2$ laser cycles and then falls as a Gaussian corresponding to the experimental pulse characterized by the FWHM duration τ_p. Although within the tunnelling picture H_2^+ appears abruptly at the peak of the laser electric field we are using a 2-cycle rise time in order to avoid the artifacts in our code which would have been induced by an abrupt turn-on of the pulse. More specifically, we use the linearly polarized (along z-axis) laser electric field in the following form

$$E(t) = \begin{cases} E_0 \sin^2[\pi t/(2t_{\rm rise})]\cos(\omega t) & \text{for } 0 < t < t_{\rm rise}, \\ E_0 \exp[-2\ln(2)(t-t_{\rm rise})^2/\tau_p^2]\cos(\omega t) & \text{for } t > t_{\rm rise}. \end{cases} \tag{5}$$

The TDSE, Eq. (1), has been solved using the wave function-splitting technique which allows to use the absorber for the electron in the internal zone defined by $|z| < z_{\rm in}$ with the absorbing zone of size z_0, see Fig. 1 in [29]. The absorber was applied at each $\delta t = 10dt$ ($dt=0.03$, $z_{\rm in}=1024$, $z_0=150$, all in a.u.) time interval. The Fourier transform in the z electron coordinate from the recovered part [given by Eq. (7) in [29]] was computed and added to that computed in the previous step. The propagation in the external zone is much faster than in the internal zone due to the Volkov propagator [see Eq. (14) in [29]]. Thus at the final simulation time t_f ($t_f \gg \tau_p$) the wave function corresponding to the external zone $\varphi(p_{\rm el},R,t_f)$ is found, where $p_{\rm el}$ is the electron momentum. In [29] $\varphi(p_{\rm el},R,t_f)$ has been projected on the nuclear plane waves $\exp(ip_N R)$ and the nuclear kinetic energy release (KER) spectra were calculated with the help of these projections. We found in [5,6] that since the nuclei at the final time t_f are only 20–40 a.u. apart it is necessary to project the final wave function on exact Coulomb wave functions instead of plane waves. Therefore, we project the final wave function $\varphi(p_{\rm el},R,t_f)$ (obtained from the recovered flux of the absorbing zone) on the Coulomb wave functions [6,30]:

$$\varphi_C(E_N,R) = \left[\frac{2\mu}{\pi k}\right]^{1/2} F_0(\eta,kR) \quad \text{where } \eta = \frac{\mu q^2}{k}, \tag{6}$$

where μ is the reduced mass of two exploding nuclei, q is a charge of each nuclei ($q=e=1$), $k=\sqrt{2\mu E_N}$ is the asymptotic momentum and F_0 is expressed by the following integral (see Eq. 14.3.3 in Ref. [30]),

$$F_0(\eta,kR) = \alpha kR \int_0^\infty dt[1-\tanh^2(t)]\cos[kR\tanh(t) - 2\eta t], \tag{7}$$

where

$$\alpha = \left[\frac{e^{2\pi\eta}-1}{2\pi\eta e^{2\pi\eta}}\right]^{1/2} \approx (2\pi\eta)^{-1/2} = \left[\frac{k}{q^2\mu}\right]^{1/2}. \tag{8}$$

The approximation made in the above equation is valid for $\eta > 3$, i.e. in the case of exploding protons for $E_N < 30$ eV, which is always satisfied in our considerations. Our choice of normalization in (6) ensures that for large R the outgoing plane wave coefficient is $\sqrt{\mu/(\pi k)}$ [i.e., the plane wave exp(ikR) is normalized to the $\delta(E-E')$ function]. The nuclear KER spectrum is thus given by

$$S(E_N) = \int_{-\infty}^{\infty} dp_{\rm el}|C(E_N,p_{\rm el})|^2,$$

$$C(E_N,p_{\rm el}) = \int_0^\infty dR\, \varphi_C^*(E_N,R)\varphi_{\rm in}(p_{\rm el},R). \tag{9}$$

Figures 2–6 show KER spectra for the wavelength $\lambda = 800$ nm obtained using the TDSE (1). In Fig. 2 we compare the experimental results with theoretical results based on the 1D (three-body) TDSE for H_2^+ and D_2^+ molecules, respectively. The numbers close to the peaks indicate possible locations $R_{\rm expl}$ (in a.u.) of Coulomb explosion if it had occurred with zero initial speed, $R_{\rm expl}=e^2/E_N$. Both, theory and experiment, show that the spacings between consecutive ex-

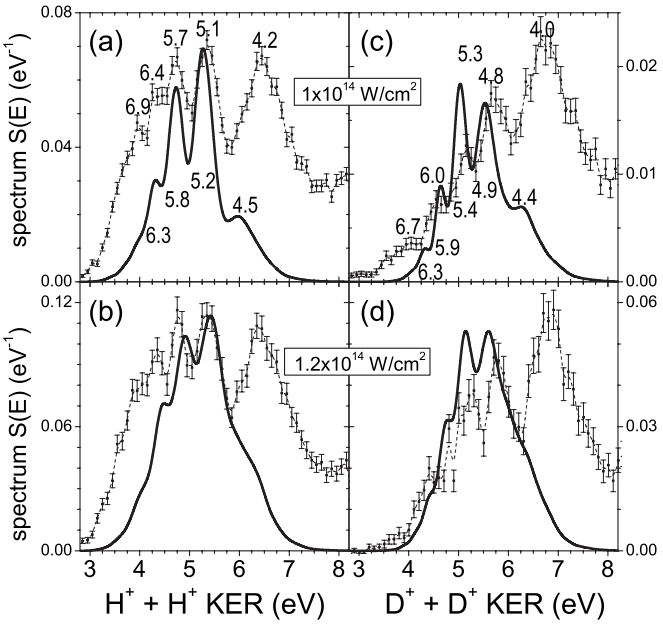

FIG. 2. Kinetic energy release (KER) spectra for H_2^+ in (a), (b) and for D_2^+ in (c), (d), as function of total ion energy calculated using the time-dependent Schrödinger equation (TDSE), given in Eq. (1), for the laser wavelength $\lambda=800$ nm, pulse duration (FWHM of the intensity profile) $\tau_p=40$ fs (solid line), compared with experimental spectra (line with symbols), at intensity (a),(c) $I=10^{14}$ W/cm^2 and (b),(d) $I=1.2\times10^{14}$ W/cm^2. Numbers near peak position indicate a possible location R_{expl} of Coulomb explosion, in a.u., calculated via $R_{\text{expl}}=e^2/E_N$.

plosion locations R_{expl} are nearly same. This suggests that the origin of the spectral lines may be related to a spatial regular structure (R-dependent). We note that the theoretical peak positions do not perfectly coincide with the experimental ones although the energy spacing between the peaks is accurately reproduced. Also, our 1D theory does not reproduce well the intensity of experimental lines. In particular, the high KER values are underestimated. Figure 6 shows that it can be partially accounted for by assuming a lower than experimental intensity. This discrepancy is probably due to the reduced dimensionality of our model calculation; note that the 1D dressed potentials exhibit the one photon crossing at $R=5.2$ a.u. and the 3-photon crossing point at $R=3.6$ a.u., whereas the corresponding exact 3-D values are smaller: 4.8 and 3.3 a.u.. This leads to the most favorable explosion conditions for 3-D model at smaller internuclear distances than in the case of a 1-D model. Fig. 3(a) also shows that the structure is more pronounced at lower intensities, $I=8\times10^{13}$ W/cm^2, and that the line progression entirely disappears in our calculations at $I=1.5\times10^{14}$ W/cm^2, see Fig. 3(b), whereas the experiment, shows a clear structure at $I=1.4\times10^{14}$ W/cm^2.

Since we have chosen an artificial pulse envelope with the two-cycle rise-time, see Eq. (5), we check in Fig. 4 the effect of the shape of the pulse envelope on the KER nuclear spectrum. Increasing the rise-time is related to assuming that the H_2^+ ion was born earlier. Clearly, the peak position depend slightly on this rise-time, however, the spacing between peaks in the KER spectra is the same for all rise-time between 2 to 8 cycles.

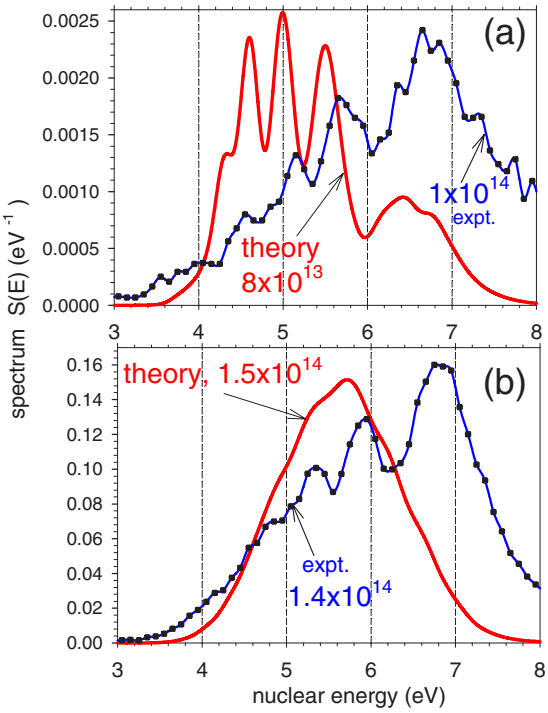

FIG. 3. (Color online) Kinetic energy release (KER) spectra for D_2^+ for laser intensity (a) $I=8\times10^{13}$ and (b) $I=1.5\times10^{14}$ W/cm^2.

Next, we check whether the peak structure in KER spectra depends on the initialization. In most previous investigations of the H_2^+ dynamics the wave function was initialized from a specific vibrational state of H_2^+. We choose the $v=6$ state of H_2^+ since the threshold for the one photon Floquet channel opens for $v\simeq6$ [31]. Thus, from $v=6$, both one and net-two-photon processes can directly occur (even at low intensities), whereas the initialization from lower vibrational states allows only for two or more photon process. We show in Fig. 5 the corresponding KER spectra for a H_2^+ molecule. Surprisingly, the line positions are identical for both, previous (Franck-Condon) and the $v=6$ state of H_2^+ initializations suggesting that the structure in the KER spectra is related to

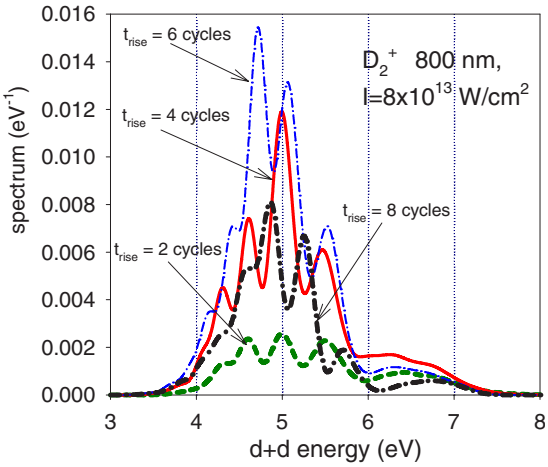

FIG. 4. (Color online) Kinetic energy release (KER) spectra for D_2^+ as function of total deuteron energy calculated using the TDSE given in Eq. (1) for several values of the pulse rise times.

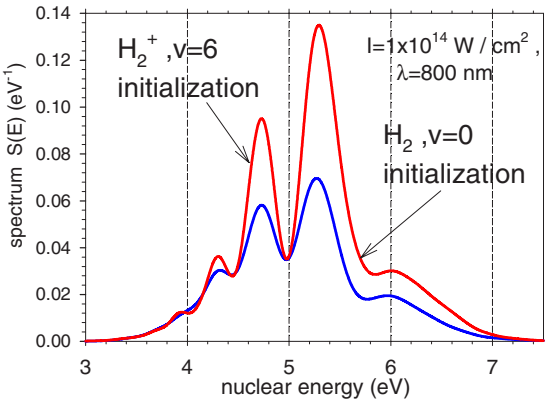

FIG. 5. (Color online) Same calculations as in Fig. 2(a) but for the H_2^+ molecule initialized in its $v=6$ vibrational state compared with the Franck-Condon initialization used in Fig. 2.

the superposition of one and two photon processes, which we will show in the next two sections.

In Fig. 6 we changed the pulse duration from $t_p=40$ fs to $t_p=80$ fs while keeping the peak intensity constant. The line intensity is shifted from the high energy lines to the lower energetic lines when the pulse duration is increased. Again, the peak positions remain unaffected. We also show in the same figure the isotope effect at $I=8\times10^{13}$ and for $t_p=80$ fs. We observe a clear isotope effect in the separation between central peaks, for D_2^+ the spacing is 0.537 eV whereas for H_2^+ the spacing is 0.353. Thus the ratio of these spacings is 1.52 which is close to the square root of reduced mass ratio, suggesting that the nuclear momentum is a parameter controlling these spacings. Clearly, the nuclear wave packet phase is responsible for this isotope effect which we will clarify in the next sections.

Figure 7 shows the nuclear KER spectra for wavelengths 1200 nm and 1400 nm. As in the case of 800 nm our simulations give correct spacing of the lines which are shifted by 0.4–0.5 eV with respect to the experimental line, most probably due to the shift of the one and three photon crossings occurring in our 1-D model. Also the intensity of lines is different from the experimental line which may be also related to our artificial preparation scheme of the molecular ion which experimentally is created by photo-ionization of a neutral molecule during the rise of the laser pulse. Comparison of the KER spectra for shorter wavelength, λ=600 nm (Fig. 8) with that for much longer wavelength, Fig. 7, shows that overall shape of KER spectra is strongly wavelength dependent: for λ=600 nm we see a strong peak at nuclear energy as high as $E_N=8$ eV which means that the Coulomb explosion already occurs at R=3.4 a.u., which is much less than the typical EI region: $6<R<11$ [11–17]. As a general rule, we observe that the spacing between peaks in our KER spectra is much smaller for λ=600 nm than for a longer wavelength. We also see a similar isotope effect for 600 nm, Fig. 8, as in the 800 nm case. Note, that in our earlier work, see Figs. 7–9 in [29], we already reported the structure in KER spectra for the wavelength λ=600 nm. However, in our current work we achieved better resolution and precision due to a longer simulation time (larger R-grids) and due to the fact that we project here the final wave function on exact Coulomb waves instead of projecting on plane waves.

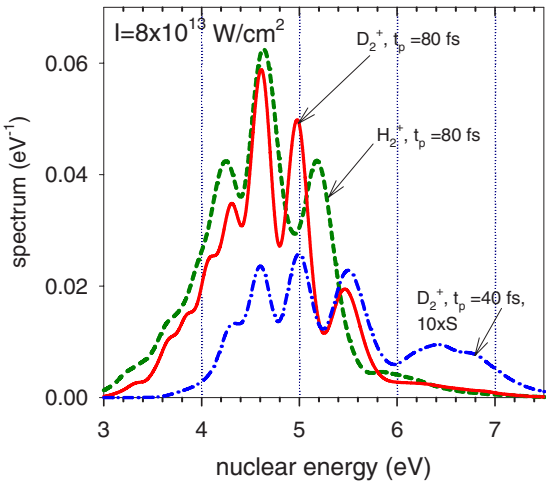

FIG. 6. (Color online) Kinetic energy release (KER) spectra for D_2^+ (solid line) compared with those for H_2^+ (dashed lines) at $I=8\times10^{13}$ W/cm^2 and for pulse duration $t_p=80$ fs, calculated using the TDSE given in Eq. (1).

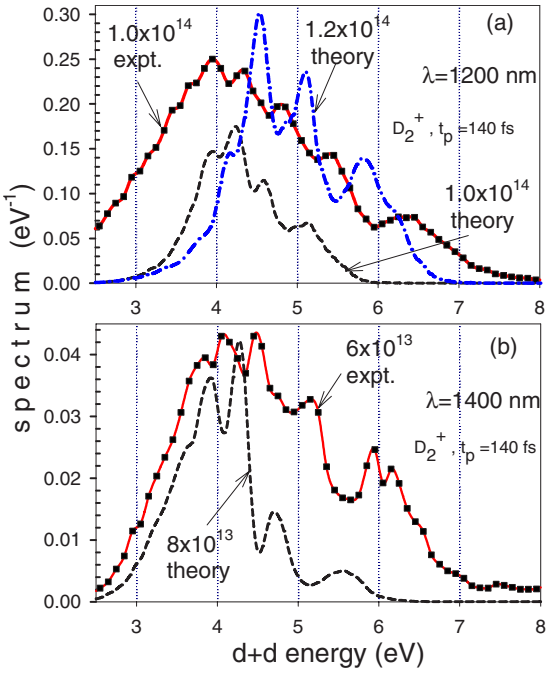

FIG. 7. (Color online) Kinetic energy release (KER) spectra for D_2^+ at wavelength λ=1200 nm calculated using the TDSE given in Eq. (1).

Summarizing, our complete simulations based on the 1-D TDSE reproduce reasonably well the spectral progression seen in the experiment, in particular the spacings between the peaks and the total number of peaks are accurately reproduced. Our simulations reproduce also the isotope dependence seen in the experiment, i.e. they show that the spacings between peaks are smaller for a heavier isotope, as well as, the dependence of peak position on the wavelength is also confirmed by theory. The dependence of the overall shape of the spectrum on the pulse duration is also similar to that seen

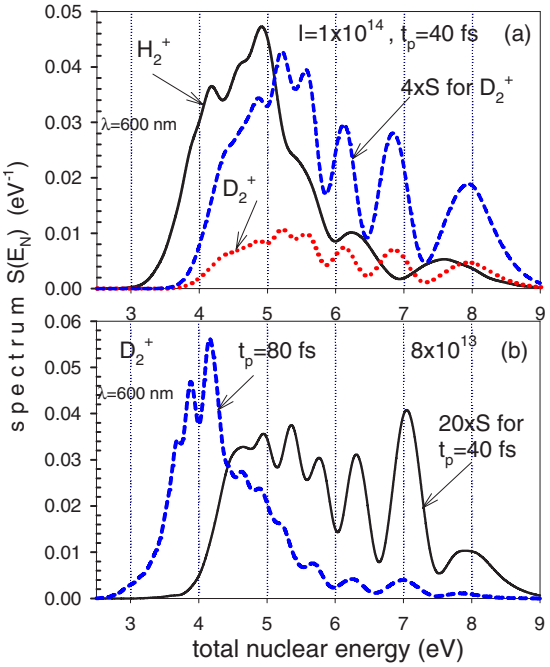

FIG. 8. (Color online) Kinetic energy release (KER) spectra for D_2^+ at wavelength $\lambda=600$ nm, calculated using the TDSE given in Eq. (1).

in the experiment. Some discrepancies in peak position between the experiment and theory are due to the reduced dimensionality of our model and initialization of the nuclear wave packet with a Franck-Condon overlap which only approximate the strong field reality involving two-electron, two nuclei dynamics.

Nevertheless, this although complete and rigorously solved model does not reveal the physical mechanism and the origin of the observed spectral progression in the KER spectra. Therefore, we present in the following two sections a model that only includes the two lowest electronic surfaces of the molecular ion, shown in Fig. 1. The nuclear wave packet is then solved rigorously. The resulting spatial shapes of the wave packet show a clear interference structure. Using this simple model we calculate the KER Coulomb explosion spectra with the help of the hypothesis that at each laser half-cycle, when the laser field reaches maximum or minimum, the instantaneous ionization occurs predominantly from a coherent nuclear wave packet on the quasi-static upper electronic surface σ_+ [13,16]; see Fig. 1. We show that the spectral lines in the KER spectra are directly linked to the spatial interference structure present in this coherent nuclear wave packet.

IV. SPATIAL INTERFERENCE STRUCTURE IN THE DISSOCIATING WAVE PACKET OBTAINED FROM THE TWO-SURFACE DYNAMICS

We model the nuclear dissociation dynamics using the two-surface TDSE in which the complete wave function $\psi(\vec{r}_{\rm el},R,t)$ is approximated as a superposition of two electronic eigenfunctions $\varphi_g^{\rm el}(\vec{r}_{\rm el},R)$ and $\varphi_u^{\rm el}(\vec{r}_{\rm el},R)$ (σ_g and σ_u) weighted by the corresponding nuclear amplitudes $\psi_g(R,t)$, $\psi_u(R,t)$ [3,24]:

$$\psi(\vec{r}_{\rm el},R,t)=\psi_g(R,t)\varphi_g^{\rm el}(\vec{r}_{\rm el},R)+\psi_u(R,t)\varphi_u^{\rm el}(\vec{r}_{\rm el},R). \quad (10)$$

Inserting the above equation into the TDSE describing the full electron-nuclear dynamics (we assume that the laser electric field is parallel to the molecular axis and limit the nuclear dynamics to 1D along z axis) yields the following two coupled differential equations for the nuclear functions $\psi_g(R,t)$, $\psi_u(R,t)$ [3]:

$$i\frac{\partial\psi_g(R,t)}{\partial t}=-\frac{1}{2\mu}\frac{\partial^2}{\partial R^2}\psi_g(R,t)+V_g(R)\psi_g(R,t)+\kappa E(t)\times\langle\varphi_g^{\rm el}|z|\varphi_u^{\rm el}\rangle\psi_u(R,t),$$

$$i\frac{\partial\psi_u(R,t)}{\partial t}=-\frac{1}{2\mu}\frac{\partial^2}{\partial R^2}\psi_u(R,t)+V_u(R)\psi_u(R,t)+\kappa E(t)\times\langle\varphi_u^{\rm el}|z|\varphi_g^{\rm el}\rangle\psi_g(R,t) \quad (11)$$

were $|\psi_g(R,t)|^2$ and $|\psi_u(R,t)|^2$ represent the probability density for the molecule in the σ_g and σ_u states, respectively, and $V_g(R)$, $V_u(R)$ are the corresponding, exact 3-D, molecular potentials. We solve these Equations numerically assuming that initially (as in the previous section) $\psi_u(R,0)=0$ and $\psi_g(R,0)$ is equal to the vibrational ground state $v=0$ of H_2 (D_2), i.e. we use the same initial condition as described by eq. (4). Eq. (11) describes correctly the dissociation dynamics of H_2^+ or D_2^+ at low intensities at which ionization occurring in one cycle is negligible. We use the same artificial laser pulse envelope as in the previous section.

The essential ingredient of our Coulomb explosion model (introduced in the next section) is an assumption that the tunnel (or overbarrier) instantaneous ionization occurs at each half-cycle of the laser field when the electric field $E(t)$ reaches maximum or minimum, $t_k=kT_{\rm las}/2$, $k=1,2,\ldots$, where $T_{\rm las}$ is the laser period. This ionization takes place from the upper quasistatic electronic state σ_+ (Fig. 1) calculated at $E(t)=E(t_k)$. This assumption is supported by Fig. 4 in [16] which shows the values of two electronic states σ_+ and σ_- of H_2^+ in the DC-electric field calculated at $E(t_k)$. Clearly, at the laser intensity $I=10^{14}$ W/cm^2 the upper (up-hill) state σ_+ is well over barrier for 4 a.u.$<R<10$ a.u., as illustrated in Fig. 1(b). Consequently, the ionization rate from this state is several order of magnitude higher [13,16,35,36] than from the down-hill σ_- state. The terms "down-hill"/"up-hill" originate from the fact that at large internuclear distance these states correspond to the well localized electrons on the left or right proton correspondingly, i.e. in order to displace the electron from its location in lower energy σ_- state into its location in the σ_+ state one moves against ("up-hill") the force originating from the laser. Hence, we believe, that ionization occurs primarily from the up-hill state and that the KER spectra are directly related to the shape of the R-dependent population $|\chi_+(R,t_k)|^2$ and to the R-dependence of the DC-ionization rates investigated earlier in [13,16,35,36].

More specifically, the electronic surface $\sigma_+(R)$ and its corresponding nuclear component $\chi_+(R,t_k)$ are calculated via diagonalization of the electronic molecular Hamiltonian with the laser interaction term $E(t)z_{\rm el}$. If we represent this Hamiltonian in the basis of just two electronic states we only need to diagonalize the following 2×2 matrix:

$$\begin{bmatrix} V_g(R) & -E(t)\mu_{g,u} \\ -E(t)\mu_{g,u} & V_u(R) \end{bmatrix}, \tag{12}$$

where $\mu_{g,u}$ is the dipole transition matrix element, $\mu_{g,u}=\langle\varphi_g^{\rm el}|z_{\rm el}|\varphi_u^{\rm el}\rangle\simeq R/2$ [3] called a charge-resonance transition [3]. The above matrix has the following eigenvalues:

$$\sigma_\pm(R,t)=\frac{1}{2}\{V_g(R)+V_u(R)\pm\sqrt{[V_u(R)-V_g(R)]^2+[E(t)R]^2}\}. \tag{13}$$

$\sigma_-(R)$ corresponds to "bond-softening" whereas $\sigma_+(R)$ leads to laser induced bound states [3,23,37,38], and is time dependent, Fig. 1(b). At large internuclear distance $R>6$ a.u. the upper $\sigma_+(R,t)$ electronic state eigenvalue simplifies to

$$\sigma_+(R,t)\simeq[V_g(R)+V_u(R)]/2+|E(t)|R/2.$$

The corresponding electronic time-dependent eigenfunction is

$$\Psi_+(\vec{r}_{\rm el},R,t)=[1+a(R,t)^2]^{-1/2}[\varphi_u^{\rm el}(\vec{r}_{\rm el},R)-a(R,t)\varphi_g^{\rm el}(\vec{r}_{\rm el},R)],$$

$$a(R,t)=\frac{RE(t)}{V_u(R)-V_g(R)+\sqrt{[V_u(R)-V_g(R)]^2+R^2E(t)^2}}. \tag{14}$$

$\Psi_+(t)$ coincides with the doorway (upper) state $\Psi_2(R,t)$ used in [22] and also called eigenfunction of the adiabatic "instantaneous" electronic Hamiltonian. In our simple Coulomb explosion model presented in the next section, we assume that the KER spectrum is directly determined via projection of the time dependent state [Eq. (10)] onto the adiabatic upper eigenstate $\Psi_+(t)$, at $t=t_k=kT_{\rm las}/2$ where $T_{\rm las}$ is the laser cycle. This projection can also be defined for any time t in the following way:

$$\chi_+(R,t)=\langle\Psi_+(t)|\psi(\vec{r}_{\rm el},R,t)\rangle$$
$$=[1+a(R,t)^2]^{-1/2}[\psi_u(R,t)-a(R,t)\psi_g(R,t)]. \tag{15}$$

Note that this is a coherent superposition of two nuclear wave functions $\psi_g(R,t)$ and $\psi_u(R,t)$. At large internuclear separations, $R>6$ a.u., and when $|E(t)|\gg V_u(R)-V_g(R)$, Eq. (15) simplifies to

$$\chi_+(R,t)\simeq 2^{-1/2}\{\psi_u(R,t)-{\rm sgn}[E(t)]\psi_g(R,t)\},$$
$${\rm sgn}[E(t)]=E(t)/|E(t)|. \tag{16}$$

Thus at $R>6$ a.u. $|\chi_+(R,t)|^2$ is the probability of finding the electron localized on the left or on the right center, depending on the changing sign of the laser field $E(t)$.

We have calculated the nuclear wave packets $\psi_u(R,t)$, $\psi_g(R,t)$ and $\chi_+(R,t)$ by solving numerically the coupled

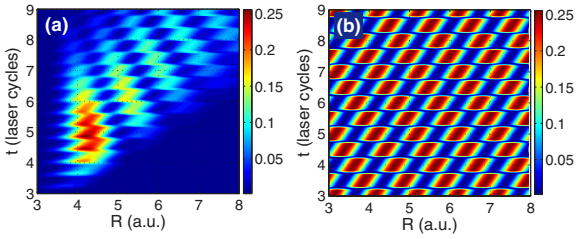

FIG. 9. (Color online) Populations $|\chi_+|^2$ on the quasistatic uphill surface on D_2^+ obtained using (a) two-surface Schrödinger equation (11) for the wavelength $\lambda=800$ nm, laser intensity $I=8\times10^{13}$ W/cm^2, $t_p=40$ fs and (b) shows $|\chi_+|^2$ calculated with the help of Eq. (16) using $E_g=1.05$ eV and $E_u=0.24$ eV.

equations (11) and using Eq. (15). We plot the resulting populations $|\chi_+(R,t)|^2$ on the up-hill surface in Fig. 9(a) which shows a very strong interference pattern. Since we expect the ionization to occur at maxima of $|E(t)|$ we examine this interference pattern in more detail by looking at populations $|\chi_+(R,t)|^2$ calculated at consecutive half-cycles, $t=7,7\frac{1}{2},8,8\frac{1}{2}\ldots$ etc. cycles, which we show separately in Figs. 10 and 11, for $\lambda=800$ nm and for $\lambda=1200$ nm, respectively. Note that we use two-cycle rise time, i.e., 7 cycles means 5 cycles after the pulse envelope reached the maximum, Eq. (5). Populations on the upper surface, shown in Fig. 9(a), appear abruptly at $t>3.5$ cycles (1.5 cycle after the pulse envelope reached a maximum. During this short time the wave packet has moved quite a large distance from $R=1.4$ a.u. (its location at t=0) to $R=4.0$ a.u. where the population was transferred up to the σ_+ surface and, surprisingly, stays constant around $R_1=4.2$ a.u. during next 3-cycles. This trapped population should lead to a clear peak in the nuclear KER spectra. If the ionization occurs at R

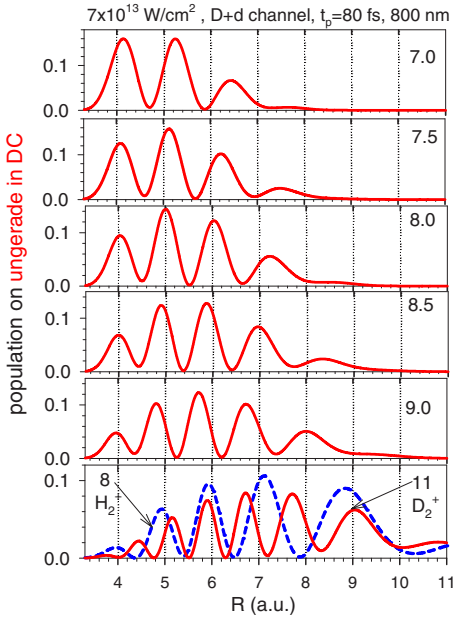

FIG. 10. (Color online) Same as in Fig. 9(a) but displayed at consecutive half-cycles, i.e., at times 7.0, 7.5, 8.0,…optical cycles T, as indicated in the right corner of each panel. $I=7\times10^{13}$ W/cm^2; $t_p=80$ fs.

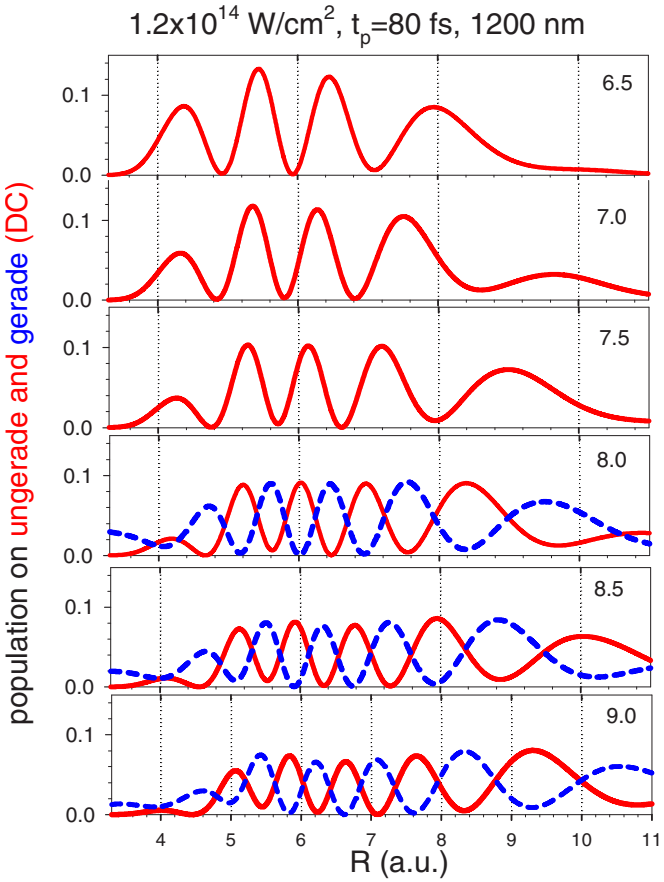

FIG. 11. (Color online) Same as in Fig. 10 but for the wavelength $\lambda=1200$ nm.

$=R_1$ the released Coulomb explosion energy is $E_{\text{expl}}=e^2/R_1=6.5$ eV which is indeed close to the highest energy peak seen in experimental spectra shown in Fig. 2(c).

In Fig. 11 we also show the population in the down-hill surface $|\chi_-(R,t_k)|^2$ (dashed line). The total population is unmodulated because the lower level has the complementary population. Both populations seem to have simple cosine like shapes shifted by $\pi/2$ with respect to each other, suggesting a simple interference mechanism taking place. Therefore, the total (incoherent) probability distribution $P(R,t)=|\chi_+(R,t_k)|^2+|\chi_-(R,t_k)|^2$ will not exhibit the interference structure.

It is surprising how wide the wave packet becomes at only $t=10$ cycles when it extends over 6 a.u. and initially its width was only 0.4 a.u.. This drastic widening of the wave packet during only a few cycles time interval tells us that the nuclear dynamics is an essential coherent factor. Consequently, static, frequency dependent rates calculated at fixed internuclear distance [11,13–18] cannot be used directly for calculations of KER Coulomb explosion spectra since even for a heavier isotope we see significant changes of the wave packet shapes in Figs. 10 and 11 occurring during few cycles. Thus, the computation of the KER should be rather done by projecting the instantaneous wave packet $\chi_+(R,t)$ at each consecutive half-cycle weighed by the ionization amplitude corresponding to each half-cycle. We present such a model calculation of KER spectra in the next section.

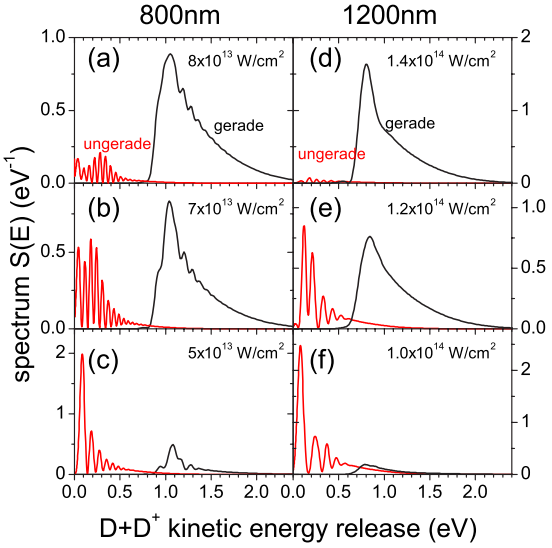

FIG. 12. (Color online) Dissociation KER in the channel $D+D^+$ calculated using two-surface Schrödinger equation (11) for (a)–(c) the wavelength $\lambda=800$ nm, and for (d)–(f), for various laser intensities given in each panel. Longer pulse duration, $\tau_p=80$ fs, is used.

The positions of peaks (and of minima) seen in Figs. 10 and 11 remain nearly unchanged within 5 to 9 laser cycles and for small internuclear separation, whereas for later times, new peaks appear at $R>6$ a.u.. The spatial position od this peaks moves to towards smaller $R's$ as function of time. The sharpness and regularity of these structures suggests that they are the direct origin of the spectral lines seen in the experimental and theoretical spectra, shown in the previous section. We already suggested earlier that the spacings between spectral depend on final nuclear momenta k_g, k_u.

In order to establish more precisely this relation we plot in Figs. 12(a)–12(c) the KER for the $D+D^+$ dissociation channel for $\lambda=800$ nm. We observe that at lower intensity, $I\ll 7\times 10^{13}$ W/cm^2, the dissociation proceeds predominantly via the ungerade σ_u surface with low energy nuclei $E_u<0.3$ eV (with one photon absorbed) whereas at higher intensities, $I\gg 7\times 10^{13}$ W/cm^2, the molecule dissociates predominantly on the gerade (σ_g surface, achieving much higher energy, $E_g\simeq 1.05$ eV. Thus, at intensities close to $7-8\times 10^{13}$ W/cm^2 we expect the strongest interference pattern since both these channels contribute nearly equally. Hence the choice of a lower laser intensity than the experimental value in Fig. 9(a) and 10 is justified in order to explore the origin of the interference phenomenon.

We now propose a very simple quantitative explanation of spacings between minima seen in Figs. 9–11. At large internuclear distance and after turning-off of the laser pulse we expect that the nuclear wave packets have the following approximate, simple (field free) form:

$$\psi_g(R,t)=a_g(R,t)\exp(ik_gR-iE_gt) \text{ and}$$

$$\psi_u(R,t)=a_u(R,t)\exp(ik_uR-iE_ut), \tag{17}$$

where $k_{g(u)}=\sqrt{2\mu E_{g(u)}}$ are the momenta of the gerade and ungerade surface and $a_{g(u)}$ are slowly varying complex func-

tions. Inserting Eq. (17) into Eq. (16) yield the following approximate shape of the coherently dissociating wave packet projected onto the up-hill quasistatic:

$$P_+(R,t) = |\chi_+(R,t)|^2 \simeq \frac{1}{2}\{|a_g|^2 + |a_u|^2 - 2\,\mathrm{sgn}[E(t)]|a_g| \times |a_u|\cos[(k_g - k_u)R - (E_g - E_u)t + \delta]\}, \quad (18)$$

where δ is the relative phase between two complex amplitudes a_g and a_u. Assuming that δ does not depend on R we conclude that for any fixed time (in particular, at each consecutive half-cycle) the function $P_+(R,t)$ has minima separated by

$$\Delta R = \frac{2\pi}{k_g - k_u}. \quad (19)$$

In Fig. 9(b) we directly plot Eq. (18) where we assumed $a_g = a_u = 1$ and $\delta = 0$ and $E_g = 1.05$ eV and $E_u = 0.24$ eV (theoretical values in Fig. 12). The resemblance of Fig. 9(b) and Fig. 9(a) at $R > 6$ a.u. constitutes a strong support for the scenario in which two waves given in Eq. (17) interfere.

We expect from Eq. (18) that the phase inside the cos-function in Eq. (18) changes by $(E_g - E_u)T_{\mathrm{las}}/2$ from one to the next half-cycle. However, since $(E_g - E_u) \simeq \omega$ this change is close to π. We also have: $E(t + T_{\mathrm{las}}/2) = -E(t)$. Consequently, if $(E_g - E_u)$ were equal to the laser frequency the positions of minima would be identical for each laser half-cycle. This simple argument explains the "stability" of the minima positions seen in Figs. 10 and 11. The slight shift to left of these minima results from the fact that $(E_g - E_u)$ is usually smaller than the photon energy. This shift to the left is clearly seen in Fig. 9(a) if we draw the lines along the minima or maxima we observe that the lines have a negative slope. Equation (18) reveals that this negative slope originates from the fact that $(E_g - E_u) < \hbar\omega$. We also checked that the lines are vertical when $(E_g - E_u) < \hbar\omega$ and the slope is positive for $(E_g - E_u) > \hbar\omega$.

Using the values of the dissociation energies, $E_g = 1.05$ eV and $E_u = 0.24$ eV we can check directly that indeed the above simple relations (19) give correct spacings between the interference minima seen in Fig. 9(a) and in Figs. 10 and 11. We thus get the corresponding values of momenta: $k_g = 11.901$ a.u., $k_u = 5.6897$ a.u., and the separation between the minima is: $\Delta R = 2\pi/(k_g - k_u) = 1.012$ a.u.. This compares well with the minima separations 1.1 a.u. seen in Fig. 10 for a D_2^+ molecule. Since the momenta $k_{g(u)}$ are proportional to the molecular reduced mass μ we expect the corresponding spacings for a H_2^+ molecule to be larger: $\Delta R = 1.431$ a.u. These estimates of the isotope effect agree with the spacings seen in the lowest panel in Fig. 10 where we superimposed the populations $|\chi_+(R,t_k)|^2$ for both isotopes. Clearly, the spacing ratio is close to the square-root of the mass ratio. Hence our simple relation (19) explains the isotope effect seen in the experimental and theoretical KER spectra, in where spacings between minima are in fact larger for H_2^+ than for D_2^+.

Similarly, since the momentum, k_g is related to the absorption of two-photons and k_u is related to the absorption of just one photon we expect k_g to be smaller for $\lambda = 1200$ nm than for $\lambda = 800$ nm, as indeed seen in Fig. 12(d)–12(f) which gives us: $E_g = 0.83$ eV and $E_u = 0.2$ eV at $I = 1.2 \times 10^{14}$ W/cm^2. Consequently, the corresponding expected spacing ΔR calculated with the help of Eq. (19) for 1200 nm is $\Delta R = 1.166$ a.u. which is larger than $\Delta R = 1.012$ a.u. for $\lambda = 800$ nm and agrees with the spacings seen in Fig. 11. Larger ΔR spacings correspond to larger separations in KER spectra (when compared within similar energy intervals) for $\lambda = 1200$ nm than for 800 nm. This is a surprising result since it is natural to expect that the separation between spectral lines is proportional to the photon energy which would lead to the smaller spacing for 1200 nm compared to 800 m. Instead, we observe the opposite effect reflecting the coherent nature of the one and two-photon absorptions. This effect is directly related to the fact that the beating between different components of the same packet slows down as as their energy difference becomes smaller with longer wavelength. Summarizing, the interference of two plane waves explains the isotope and wavelength dependence of the peak spacings.

V. SIMPLE MODELS OF THE DISSOCIATIVE IONIZATION FROM THE UPHILL QUASISTATIC SURFACE

We now introduce a simple Coulomb explosion model based on coherent dissociating wave packets $\chi_+(R,t)$ [defined in Eq. (15)] obtained numerically from the two-surface model described in the previous section. The model relies on the assumption that at each consecutive minimum and maximum of the laser electric field $E(t)$, i.e., at $t = t_k = kT_{\mathrm{las}}/2$, a fraction of the nuclear wave packet χ_+ is transferred instantaneously from the quasi-static surface σ_+ onto the $p+p$ (or $d+d$) repulsive $p+p$ (or $d+d$) surface. The nuclear eigenfunctions $\varphi_C(E_N,R)$ on this repulsive surface are given in eq. (6). Subsequent contributions to the instantaneous Coulomb explosion from each consecutive half-cycle are added incoherently as a sum of transition probabilities to the $p+p+e$ continuum states. Let us assume that the amplitude for for this instantaneous electronic jump occurring at fixed internuclear separation R, at $E(t) = E(t_k)$ is $B_{\mathrm{el}}(\vec{p}_{\mathrm{el}}, R, E(t_k))$. Assuming that the initial and final wave functions are proportional to the "pure" (i.e. only R-dependent) nuclear wave functions $\chi_+(R,t_k)$ and $\varphi_C(E_N,R)$ we calculate the nuclear spectra $S(E_N)$ (integrated over the electronic momenta $\vec{p}_{\mathrm{el}}$) in the following way:

$$S(E_N) = \sum_{k=1}^{k_f} \int d^3p_{\mathrm{el}} |A(\vec{p}_{\mathrm{el}}, E_N, E(t_k))|^2, \quad (20)$$

where

$$A(\vec{p}_{\mathrm{el}}, E_N, E(t_k)) = \int_0^\infty dR\, B_{\mathrm{el}}(\vec{p}_{\mathrm{el}}, R, E(t_k))\varphi_C^*(E_N,R)\chi_+(R,t_k) \quad (21)$$

is the transition amplitude (at instantaneous field $E(t_k)$) from the initial state $\Psi_+(\vec{r}_{\mathrm{el}}, R, t)\chi_+(R,t_k)$ into the final free elec-

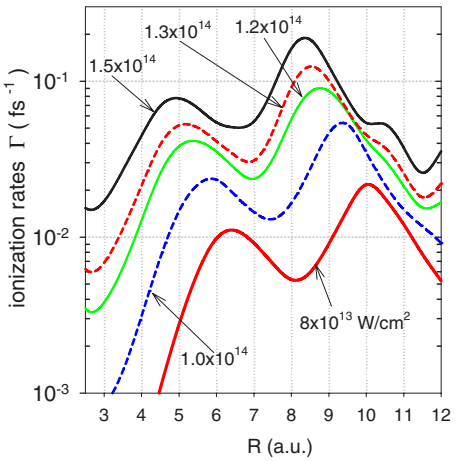

FIG. 13. (Color online) Ionization rates Γ in the dc-electric field obtained from Tables 1 and 2 in [35].

tron state characterized by the momentum $\vec{p}_{\rm el}$ and free $p+p$ (or $d+d$) state having the kinetic energy E_N and described by $\varphi_C(E_N,R)$, where $\Psi_+(\vec{r}_{\rm el},R,t)$ was defined in Eq. (15). Knowing that the Coulomb wave function $\varphi_C(E_N,R)$ is well localized at $R \simeq R_{\rm expl}=e^2/E_N$ [5] (in fact, standard Coulomb explosion imaging relies on replacing the Coulomb wave function by the Dirac $\delta(R-e^2/E_N)$ function) we expect that the function $B_{\rm el}(\vec{p}_{\rm el},R,E(t_k))$ varies little in comparison with $\varphi_C(E_N,R)$ and therefore it can be extracted outside the integral with the substitution $R=e^2/E_N$. This leads us to the model I (which was already used earlier in [21]):

$$S_I(E_N)=\sum_{k=1}^{k_f}|f_k^{\rm FC}|^2|P_k(R)|_{R=e^2/E_N}, \tag{22}$$

where the value of the index k_f is fixed by the requirement that the summation stops when the laser intensity $I(t)$ falls to $I_{\max}/8$. In Eq. (22)

$$f_k^{\rm FC}=\int_0^\infty \Psi_C(E_N,R')\chi_+(R',t_k)dR' \tag{23}$$

are the Franck-Condon factors for the transition from the quasistatic σ_+ surface $f_k^{\rm FC}$ to the $p+p$ (or $d+d$) repulsive surface and

$$P_k(R)=\int d^3p_{\rm el}|B(\vec{p}_{\rm el},R,E(t_k))|^2 \text{ at } R=e^2/E_N \tag{24}$$

are the ionization probabilities which we calculate using published ionization rates $\Gamma(R,E(t_k))$ (averaged over a half-cycle) from the upper state $\Psi_+(R,t_k)$ given in Tables 1, 2 in [35]. We plot these rates in Fig. 13. The probabilities $P_k(R)$ are calculated in the following way:

$$P_k(R)=1-\exp[-\Gamma(R,E(t_k))T_{\rm las}/2] \text{ at } R=e^2/E_N. \tag{25}$$

Model I was derived with the help of the assumption that the variation of the electronic amplitude $B_{\rm el}(\vec{p}_{\rm el},R,E(t_k))$ is negligible in comparison with the variation $\varphi_C(E_N,R)$ and therefore we extracted the amplitude $B_{\rm el}$ outside the integral present in Eq. (21). However, we conclude from Fig. 13 that

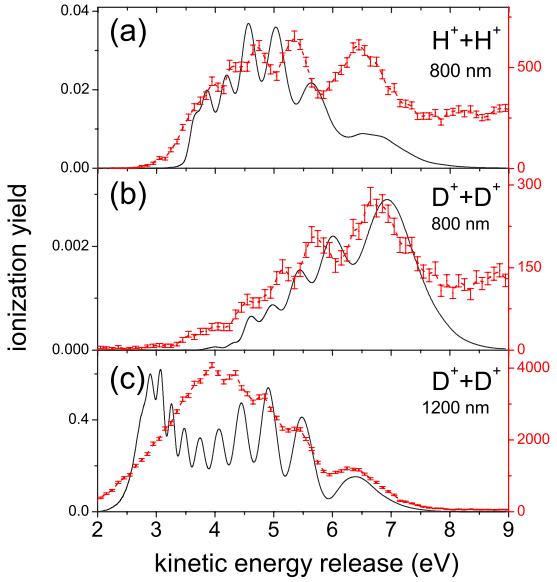

FIG. 14. (Color online) KER nuclear spectra obtained using model I described by Eq. (22).

at intensities $I<10^{14}$ W/cm^2 and at $R<4.5$ a.u. the ionization rates $\Gamma(R)$ vary rapidly.

We propose model II which takes into account approximately the R dependence of $B_{\rm el}$ inside the integral present in Eq. (21). Since we do not know the complex amplitude $B_{\rm el}(\vec{p}_{\rm el},R,E(t_k))$ we extract from it its fast varying factor $P_k(R)$ obtained after the integration of $|B_{\rm el}|^2$ over the electron momenta, i.e. we write this amplitude in the form:

$$B_{\rm el}(\vec{p}_{\rm el},R,E(t_k))=\sqrt{P_k(R)}\frac{B_{\rm el}(\vec{p}_{\rm el},R,E(t_k))}{\sqrt{P_k(R)}}. \tag{26}$$

We now retain the first factor $P_k(R)$ from the above equation inside the integral present in Eq. (21) and extract outside this integral the factor $B_{\rm el}/\sqrt{P_k}$. We expect that the latter factor variation as function of R is slower than the variation of $P_k(R)$. This leads us to model II described by

$$S_{\rm II}(E_N)=\sum_{k=1}^{k_f}|f_k'^{\rm FC}|^2, \tag{27}$$

where

$$f_k'^{\rm FC}=\int_0^\infty \Psi_C(E_N,R)\sqrt{P_k(R)}\chi_+(R,t_k)dR. \tag{28}$$

This model resembles a model used earlier in [9,10] for the first step ionization of H_2, where the variation due to ionization rates was introduced inside the Franck-Condon factor for transition from the $v=0$ state of H_2 to the vibrational states of H_2^+.

In Fig. 14 we compare the results of our model I with the experimental data. Sampling each 1/2 laser period by field ionization and adding incoherently, as described in Eq. (22) we obtain a reasonably good agreement of the peak spacing with the experiment. We note, by comparing Fig. 14(a) with Fig. 14(b) that the isotope effect seen in the experiment is

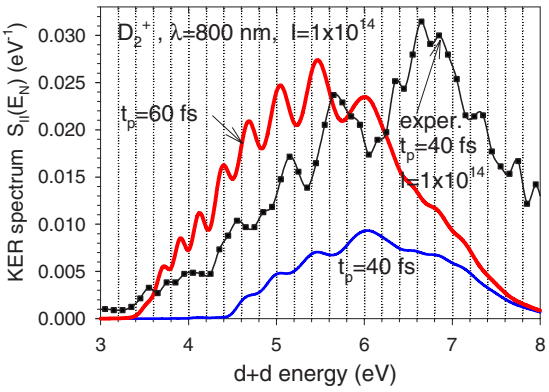

FIG. 15. (Color online) KER nuclear spectra obtained using model II described by Eq. (27).

correctly reproduced by our simple model. For the case of wavelength $\lambda=800$ nm, we note a systematic shift of theoretical peaks compared to the experimental one which originates probably from the simplicity of our model which does not describe properly the initial (involving two-electron effect) part. Note, however, that for the longer wavelength case, $\lambda=1200$ nm, the experimental and theoretical peak positions are very close one to another. Furthermore, by comparing Fig. 14(b) with Fig. 14(c) we confirm the general trend in wavelength dependence of peak spacings in the KER nuclear spectra.

Despite the conceptual improvement model II yields worse agreement with the experiment, see results for the pulse duration $t_p=40$ fs, for which the spectrum exhibit nearly no oscillations. The oscillations appear for longer, $t_p=60$ fs pulses, but the high energy tail ($E_N>5$ eV) differs significantly from the experimental results. We suspect that this negative result is related to the fact that at an intensity $I=10^{14}$ W/cm^2 the ionization probability strongly suppresses the wave packet part for $R<4.5$ a.u.; see Fig. 13. By using higher intensity one allows to conserve the full shape of the wave packet during the projection process onto the repulsive Coulomb $p+p$ (or $d+d$) surface. But at the same time, the use of higher intensities leads to the destruction of the interference pattern which we believe originates from the interplay between two dissociation channels leading to two distinct dissociation peaks in the $H+p$ (or $D+d$) channel.

This observation suggests to introduce model III, which takes into account the fact that part of the spectrum may originate from non-aligned molecules which "feel" weaker electric field than molecules whose axis are perfectly parallel to the laser polarization. Note that models I and II assume that all molecules are perfectly aligned with the linearly polarized laser field, whereas ionization of H_2 occurs from an isotropic ensemble leading to the creation of H_2^+ molecules with a small degree of alignment. The possible importance of this nonalignment effect is indeed supported by angle resolved experimental KER shown in Fig. 16, where angle θ is an angle between the molecular axis and the laser polarization. In Fig. 16 we examine the experimental distribution of deuterons in the laboratory frame in linearly polarized, 800 nm laser pulses of 40 fs duration at a peak intensity of 1.4×10^{14} W/cm^2. Only deuterons produced by enhanced ionization of D_2 are included. Figure 16(a) shows the momentum components along the laser polarization and along the axis of the gas jet. Clearly, not all molecules are perfectly aligned with the polarization. Therefore, a considerable fraction of the molecules experiences a decreased laser field strength along the molecular bond. Figure 16(b) plots the kinetic energy release of exploding molecules versus the polar angle of the molecular axis with respect to the laser polarization. We then make cuts for different solid angle intervals and project the corresponding kinetic energy release as shown in Fig. 16(c). The fixed binning size of the solid angle is responsible for the seemingly vanishing ionization yield for almost perfectly aligned molecules. Consequently, the maximum number of counts $N_{\max}$ peaks for the solid angle interval of 11°–20° [see line labels in Fig. 16(c)]. Strikingly, the peak position seems to be dependent on the angle between molecule and laser field, i.e., better alignment shifts the peaks to lower energies. At angles larger than 40° structure in the enhanced ionization cannot be found. We also note, the peaks from the interval of rather large angles, 21°–40° and from the interval 11°–20° are sharper than from smallest angle interval. This is probably related to the fact that the nonaligned molecules dissociate in the weaker field, since the field component along the molecular axis is $E(t)\cos(\theta)$, and the weaker field should lead to stronger interference structure as expected from the discussion in previous section related to Fig. 12.

We investigate in model III these rotational effects by choosing an angle $\theta=35°$ in the dissociation step, i.e., we perform the dissociation simulation based on Eq. (11) in which $E(t)$ is replaced by $E(t)\cos(\theta)$. We assume, however, that the ionization occurs at the full field value, i.e., it is assumed that the Coulomb explosion rate from the "up-hill" state is angle independent. This scenario accounts for the different alignment sensitivities of the dissociation and ionization steps, clearly, the dissociation cannot occur (within our two-surface model) at an angle $\theta=90°$ while ionization is possible at this angle. We may also expect that during the wave packet motion from $R=R_{\rm eq}=1.4$ a.u to the critical EI distance $R=R_C\simeq5-10$ a.u. the molecular ions become better aligned with the field.

We show in Fig. 17 spectra obtained using the model III for $\theta=35°$, and for an intensity $I=1.2\times10^{14}$ W/cm^2, the latter is slightly higher than the experimental intensity. We note a much better agreement between theory and the experiment for a H_2^+ molecule and only slight improvement of theoretical peak position for D_2^+ molecule (with respect to model I). However, for the wavelength $\lambda=1200$ nm at an intensity $I=1.5\times10^{14}$ W/cm^2, the model III agrees very well with the experimental spectra (see Fig. 18.)

Our studies of the wave packet spatial shapes presented in the previous section suggest that the regular spectral progression seen in the KER spectra may originate from the interference of two wave packet having two, rather well defined momenta k_g and k_u. In order to demonstrate directly this link we performed a series of calculations based on the model III in which we altered the two-surface dissociation dynamics by removing the populations on the ungerade surface at a series of chosen intervals $R<R_{\rm cut}$. Starting from $R_{\rm cut}=3.3$ a.u. we remove the contribution from the three-photon

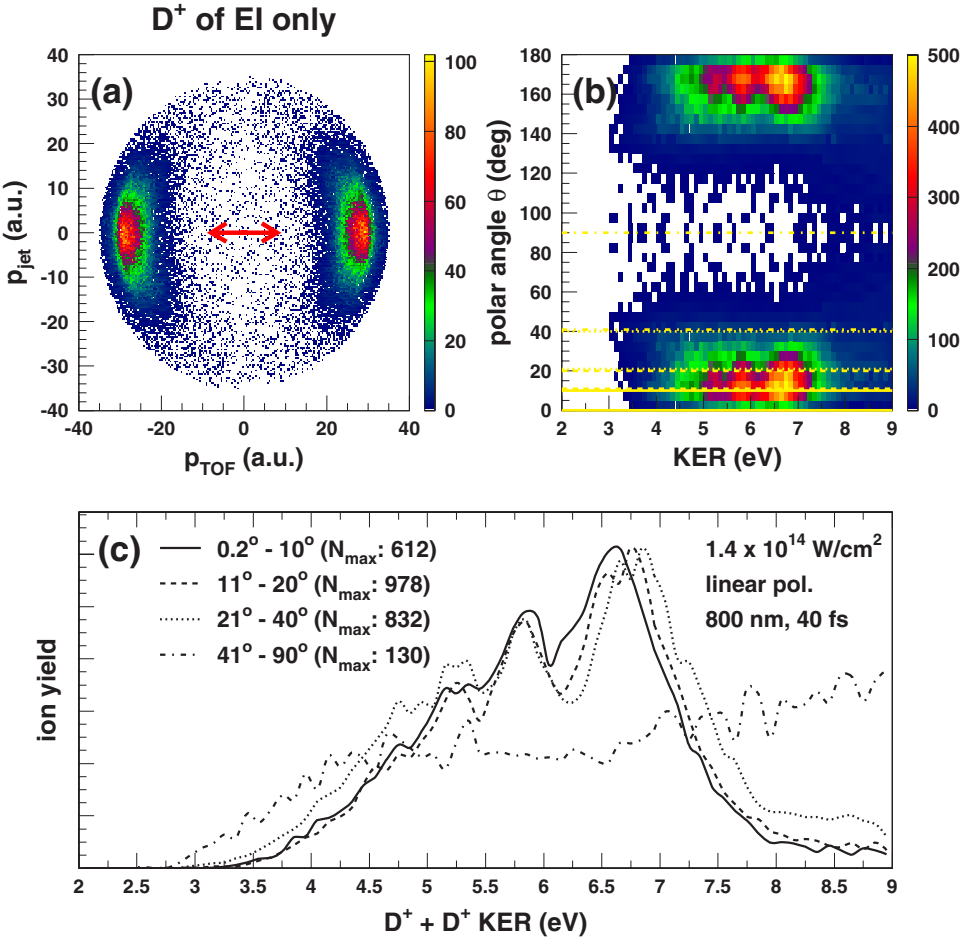

FIG. 16. (Color online) Momentum and angle resolved experimental KER spectra. Panel (a): Experimental distributions of deuterons produced by enhanced ionization (EI) at the laser parameters indicated in (c). The polarization is horizontal. Panel (b) Same data as in (a), but different presentation. Kinetic energy release of deuteron pairs in the EI region vs the angle θ between the molecular axis and polarization. Horizontal lines indicate position of angular intervals projected in panel (c). Panel (c): Projection of angular intervals. Number of maximum counts $N_{\max}$ for each projection is given in the figure.

crossing. For $R=R_{\rm cut}\simeq 4.4$ a.u. we eliminate the net-two-photon contribution which occurs via the intermediate σ_u state. The results presented in Fig. 19 and also in Fig. 20 (for model I and very low intensity) demonstrate that by increasing, step by step, the cutting interval defined by $R_{\rm cut}$ we gradually decrease the amplitude of oscillation in the spectral progression. When the transitions occur only close to the one-photon crossing (which occurs at $R=4.8$ a.u.) the structure vanishes in the spectrum. More specifically, we see in Fig. 20 that if we remove a part of the wave packet corresponding to the first maximum in $R=4.2$ a.u seen in Fig. 9(a) the interference is removed. This proves that the fast component of the wave packet $\chi_+(R,t)$ created at $R\simeq 4.2$ a.u. [see Fig. 9(a)] is essential in the interference process. Clearly, the origin of the lines has thus a rather dynamical character, since when the wave packet is prepared only via an one-photon crossing (thus it has only a low momentum k_u component) the structure vanishes.

Finally, since we have used an artificial pulse envelope, see Eq. (5), we have checked using model I the sensitivity of the model spectra to the rise time $t_{\rm rise}$. We observed that the peak position remains unchanged for $t_{\rm rise}=1$ and 0.5 cycle. The sensitivity of spectra to pulse rise (for longer $t_{\rm rise}$) was also checked with the help of our TDSE code; see Fig. 4.

Summarizing, we have established the origin of the modulation on the two surfaces. From Eq. (16) we expect that effectively two coherent plane waves will interfere leading to the appearance of a cosine like structure in $|\chi_+(R)|^2$

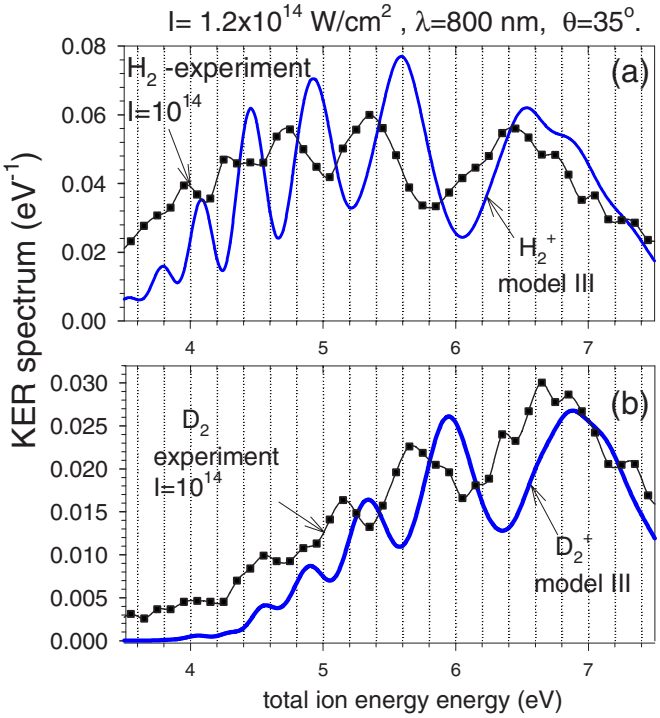

FIG. 17. (Color online) KER nuclear spectra obtained using model III described by Eq. (27) using an angle $\theta=35°$ and a laser intensity $I=2\times 10^{14}$. Wavelength $\lambda=800$ nm and pulse duration $t_p=40$ fs are used.

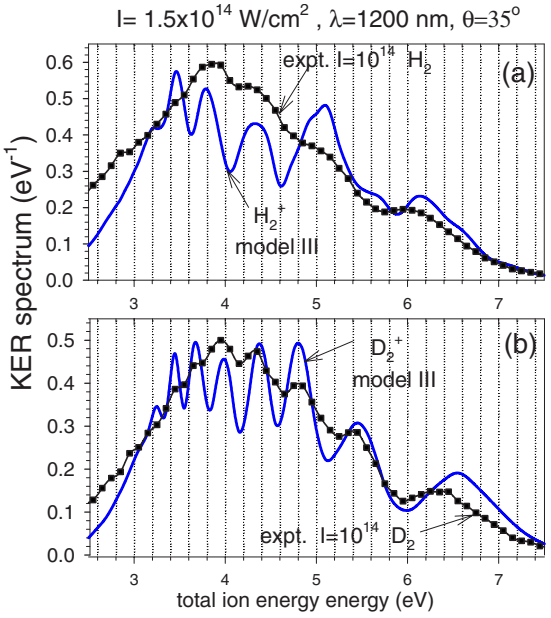

FIG. 18. (Color online) KER nuclear spectra obtained using model III described by Eq. (27) using an angle $\theta=35°$ at laser intensity $I=1.5\times10^{14}$. Wavelength $\lambda=1200$ nm and the pulse duration $t_p=140$ fs are used.

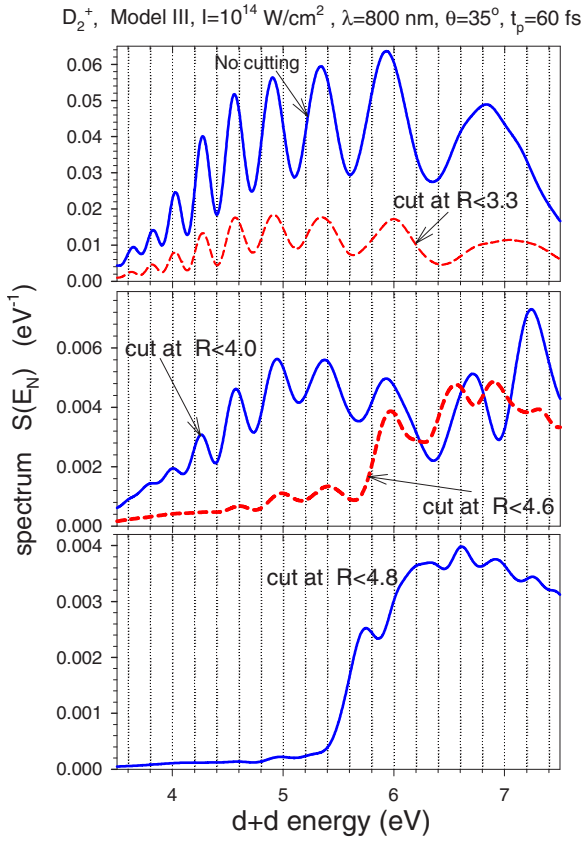

FIG. 19. (Color online) Investigations of the effect of cutting populations at $R<R_{\mathrm{cut}}$ for a series of R_{cut} values using the same model as in Fig. 17 with the same angle $\theta=35°$ but for a laser intensity $I=1\times10^{14}$. Wavelength $\lambda=800$ nm is used.

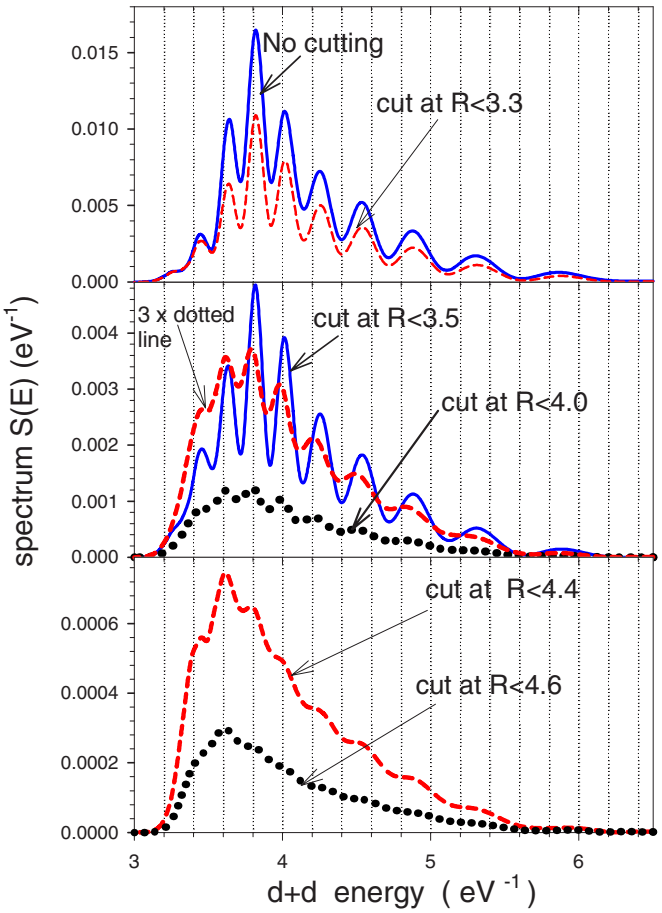

FIG. 20. (Color online) Same investigations as in the previous figure but using the model I for $I=7\times10^{13}$ W/cm^2, wavelength $\lambda=800$ nm, and $t_p=80$ fs.

and in the Franck-Condon factor present in Eq. (22). This interference leads to the minima in the probability shape $|\chi_+(R)|^2$ separated by $2\pi/(k_g-k_u)$ which are close to the experimental separations and this simple relation accounts well for the isotope and wavelength dependence of the experimental spectral progression. Thus we arrive at the conclusion that the regular structures observed in the Coulomb explosion spectra originate from the interference of nuclear wave packets corresponding to the net-two-photon with one-photon channels; see Eqs. (15) and (18).

The intensity dependence is explained naturally: At higher intensity the relative strength of the two dissociation channels becomes disparate. In fact, one would expect that the interference disappears at very low intensity when the net-two-photon channel is closed. However, at these intensities double ionization is also strongly suppressed obstructing a possible experimental detection.

VI. CONCLUDING REMARKS

In conclusion, the experiment reported in [21] revealed an important phenomenon: In the presence of an intense laser pulse, the electron population on the quasistatic upper potential energy surface σ_+ of dissociating H_2^+ and D_2^+ has a

strong *R*-dependent modulation. The total population is unmodulated because the lower level has the complementary population. It is the spatial equivalent of a two-level system where the population is transferred between the upper and lower state during Rabi oscillations, but the total population is fixed. We expect similar *R*-dependent population dynamics to occur in other dissociating molecules or during photoassociation of cold atoms during cold molecule formation.

We obtained quantitative reasonable agreement between theory and experiment using two theoretical models: The first was based on the TDSE describing 1D three body ($p+p+e$) dynamics and in the second the molecular dissociation dynamics was modelled using a two-surface model for H_2^+ sampled by ionization at the peak of the field with an ionization rate taken from preceding work. Thus, with the help of the latter model, we established the origins of the modulation in the two-surface dynamics of dissociating H_2^+ (D_2^+). It reflects a previously unrecognized regular spatial structure of the electronic excitation in the quasistatic upper state σ_+ of the molecular ion. It appears that the probability of finding the electron localized on a specific nucleus is strongly dependent on the internuclear separation *R* and is closely related to the final momenta of dissociating fragments. Next, using simple model for Coulomb explosion we showed these modulated populations are being sampled by field ionization twice per laser period with a 360 as (800 nm)-620 as (1400 nm) sampling window (FWHM of the tunnelling rate as function of time within each half-cycle). Coulomb explosion occurring at each consecutive half-cycle reveals the *R*-dependent structure. Summarizing, our work completes previous investigations of enhanced ionization which focused on *R*-dependent rates obtained with the help of TDSE for H_2^+ at fixed internuclear distance *R* without providing an appropriate link between the frequency dependent ionization rates and the KER nuclear spectra. Another surprising result of our investigation is the observation of the unexpectedly wide nuclear wave packet. Its width (over 6 a.u.) suggests that it is rather inadequate to describe the nuclear motion classically using the *R*-dependent localized trajectories in light molecular system such as H_2^+ or D_2^+.

ACKNOWLEDGMENTS

We gratefully acknowledge stimulating discussions with D. M. Villeneuve, R. Dörner, C. L. Cocke, and H. Kono. The experimental work was supported by an NSERC accelerator grant, NSERC Centre-of-Excellence for Photonic Innovation, NRC HGF science and technology fund, DFG, Alexander-von-Humboldt Stiftung and the Studienstiftung des deutschen Volkes. The theoretical work was funded by NSERC and by CIPI. We also thank the Maui High Performance Computing Center (Hawaii) for the access to their computers where most numerical simulations were performed.

[1] H. Niikura and P. B. Corkum, Adv. At., Mol., Opt. Phys. **54**, 511 (2007).
[2] *Atoms in Laser Fields*, edited by M. Gavrila (Academic Press, San Diego, 1992).
[3] *Molecules in Intense Laser Fields*, edited by A. D. Bandrauk (Marcel Dekker, New York, 1994).
[4] A. Zavriyev, P. H. Bucksbaum, H. G. Muller, and D. W. Schumacher, Phys. Rev. A **42**, 5500 (1990).
[5] S. Chelkowski, P. B. Corkum, and A. D. Bandrauk, Phys. Rev. Lett. **82**, 3416 (1999).
[6] S. Chelkowski and A. D. Bandrauk, Phys. Rev. A **65**, 023403 (2002).
[7] H. Stapelfeldt, E. Constant, and P. B. Corkum, Phys. Rev. Lett. **74**, 3780 (1995); H. Stapelfeldt, H. Sakai, E. Constant, and P. B. Corkum, Phys. Rev. A **55**, R3319 (1997).
[8] F. Légaré, K. F. Lee, I. V. Litvinyuk, P. W. Dooley, A. D. Bandrauk, D. M. Villeneuve, and P. B. Corkum, Phys. Rev. A **72**, 052717 (2005).
[9] X. Urbain, B. Fabre, E. M. Staicu-Casagrande, N. de Ruette, V. M. Andrianarijaona, J. Jureta, J. H. Posthumus, A. Saenz, E. Baldit, and C. Cornaggia, Phys. Rev. Lett. **92**, 163004 (2004).
[10] A. Requate, A. Becker, and F. H. M. Faisal, Phys. Rev. A **73**, 033406 (2006).
[11] J. Posthumus, L. Frasinski, A. Giles, and K. Codling, J. Phys. B **28**, L349 (1995).
[12] K. Codling and L. Frasinski, J. Phys. B **26**, 783 (1993).
[13] T. Zuo and A. D. Bandrauk, Phys. Rev. A **52**, R2511 (1995).
[14] T. Seideman, M. Y. Ivanov, and P. B. Corkum, Phys. Rev. Lett. **75**, 2819 (1995).
[15] S. Chelkowski and A. D. Bandrauk, J. Phys. B **28**, L723 (1995).
[16] A. D. Bandrauk and H. Z. Lu, Phys. Rev. A **62**, 053406 (2000).
[17] H. Sabzyan and M. Vafaee, Phys. Rev. A **71**, 063404 (2005).
[18] G. L. Kamta and A. D. Bandrauk, Phys. Rev. Lett. **94**, 203003 (2005).
[19] G. N. Gibson, M. Li, C. Guo, and J. Neira, Phys. Rev. Lett. **79**, 2022 (1997).
[20] B. D. Esry, A. M. Sayler, P. Q. Wang, K. D. Carnes, and I. Ben-Itzhak, Phys. Rev. Lett. **97**, 013003 (2006).
[21] A. Staudte, D. Pavičić, S. Chelkowski, D. Zeidler, M. Meckel, H. Niikura, M. Schöffler, S. Schössler, B. Ulrich, P. P. Rajeev, Th. Weber, T. Jahnke, D. M. Villeneuve, A. D. Bandrauk, C. L. Cocke, P. B. Corkum, and R. Dörner, Phys. Rev. Lett. **98**, 073003 (2007).
[22] H. Kono, Y. Sato, Y. Fujimura, and I. Kawata, Laser Phys. **13**, 883 (2003).
[23] A. Zavriyev, P. H. Bucksbaum, J. Squier, and F. H. Saline, Phys. Rev. Lett. **70**, 1077 (1993).
[24] T. D. G. Walsh, F. A. Ilkov, S. L. Chin, F. Châteauneuf, T. T. Nguyen-Dang, S. Chelkowski, A. D. Bandrauk, and O. Atabek, Phys. Rev. A **58**, 3922 (1998).
[25] A. S. Alnaser, X. M. Tong, T. Osipov, S. Voss, C. M. Maharjan, B. Shan, Z. Chang, and C. L. Cocke, Phys. Rev. A **70**,

023413 (2004).
[26] A. Staudte, Ph.D. thesis, J. W. Goethe Universität, Frankfurt/Main, www.atom.uni-frankfurt.de (2005).
[27] S. Chelkowski, T. Zuo, O. Atabek, and A. D. Bandrauk, Phys. Rev. A **52**, 2977 (1995).
[28] S. Chelkowski, A. Conjusteau, T. Zuo, and A. D. Bandrauk, Phys. Rev. A **54**, 3235 (1996).
[29] S. Chelkowski, C. Foisy, and A. D. Bandrauk, Phys. Rev. A **57**, 1176 (1998).
[30] *Handbook of Mathematical Functions*, edited by M. Abramowitz and I. R. Stegun (Dover, New York, 1972), Eq. 14.3.3.
[31] B. Feuerstein and U. Thumm, Phys. Rev. A **67**, 043405 (2003).
[32] A. S. Alnaser, T. Osipov, E. P. Benis, A. Wech, B. Shan, C. L. Cocke, X. M. Tong, and C. D. Lin, Phys. Rev. Lett. **91**, 163002 (2003).
[33] H. Niikura, F. Légaré, R. Hasbani, A. D. Bandrauk, M. Ivanov, D. Villeneuve, and P. Corkum, Nature (London) **417**, 917 (2002).
[34] S. Chelkowski, M. Zamojski, and A. D. Bandrauk, Phys. Rev. A **63**, 023409 (2001).
[35] M. Plummer and J. McCann, J. Phys. B **29**, 4625 (1996).
[36] Z. Mulyukov, M. Pont, and R. Shakeshaft, Phys. Rev. A **54**, 4299 (1996).
[37] A. D. Bandrauk and M. L. Sink, J. Chem. Phys. **74**, 1110 (1981).
[38] A. Giusti-Suzor and F. H. Mies, Phys. Rev. Lett. **68**, 3869 (1992).